Applied Catalysis B: Environmental 309 (2022) 121224

Contents lists available at ScienceDirect

Applied Catalysis B: Environmental

journal homepage: www.elsevier.com/locate/apcatb

Confinement and synergy effect of bimetallic Pt-Mn nanoparticles encapsulated in ZSM-5 zeolite with superior performance for acetone catalytic oxidation

Lizhe Yang [a,b], Qingling Liu [a,b,*], Rui Han [a,b,*], Kaixuan Fu [a,b], Yun Su [a,b], Yanfei Zheng [a,b], Xueqian Wu [a,b], Chunfeng Song [a,b], Na Ji [a,b], Xuebin Lu [a,b], Degang Ma [a,b]

[a] Tianjin Key Lab of Indoor Air Environmental Quality Control, School of Environmental Science and Technology, Tianjin University, Tianjin 300350, China
[b] State Key Laboratory of Engines, School of mechanical engineering, Tianjin University, Tianjin 300350, China

ARTICLE INFO

Keywords:
VOCs oxidation
Catalyst
Zeolite
Confinement
Bimetal

ABSTRACT

Catalytic oxidation is one of the most promising methods to remove VOCs. Herein, a zeolite-confined PtMn bimetal catalyst ($PtMn_{0.2}$ @ZSM5) was synthesized using a ligand-assisted hydrothermal method, which showed extraordinary catalytic activity with a T_{95} of 165 °C for the acetone oxidation in the presence of 5 vol% water. Thanks to the zeolite confinement and bimetallic synergy effect, the $PtMn_{0.2}$ @ZSM5 exhibited small nanoparticle sizes, abundant acid sites, higher active Pt^0 content, and sufficient active oxygen species. These excellent properties promoted the adsorption of VOC, the deep oxidation of VOC, and the desorption of CO_2. In-situ DRIFTS proposed an L-H mechanism for acetone oxidation over $PtMn_{0.2}$ @ZSM5. Significantly, the $PtMn_{0.2}$ @ZSM5 presented good durability and water resistance under high GHSV conditions. Also, it was confirmed effective for various VOCs oxidation, such as toluene, ethyl acetate, propane, and dichloromethane, showing a promising industrial prospect for eliminating VOCs.

1. Introduction

Volatile organic compounds (VOCs) are a category of environmental pollutants that can promote suspended particulates, ozone, and photochemical smog. Threats to human health from VOCs have also been documented [1,2]. In the case of severe VOCs pollution, many technologies have been developed to deal with VOCs abatement [3–6]. Catalytic oxidation is recognized as one of the most promising VOCs treatment methods due to its economic viability, high efficiency, and harmless products [3,7].

There are two major types of catalysts for VOCs oxidation: supported noble metal catalysts (SNMCs) and transition-metal oxides (TMOs). Despite the higher cost, the SNMCs are generally preferred due to their excellent activity, especially the Pt-based catalysts [8]. However, the catalytic performance of SNMCs is significantly influenced by many factors, such as the loading content, size, dispersion, and interaction with supports [9–11].

As a commonly used support of noble metals, zeolite has well-defined microporous structures, outstanding thermal stability, and tunable acidity [12], attracting much attention in the field of adsorption and catalysis. However, conventional zeolite-supported metals tend to suffer from agglomeration under harsh conditions because of the limited metal-support interaction [13,14], thus leading to deactivation and increasing the economic cost. To achieve long-term stability and high efficiency in applications, a type of zeolite-confined metal catalysts (metal@zeolite) is proposed [15,16]. Due to the confined effect by the rigid framework and enhanced support-metal interaction, the metal nanoparticles inside zeolite are inhibited from migrating [17]. Moreover, the confined metal nanoparticles are close to the acid sites of zeolite, which strongly affect zeolite's acidic property and microenvironment [18,19]. As a result, there may be a pronounced synergy between these two kinds of active sites. Some typical metal@zeolite catalysts (Pt@MFI [20], Pd@MFI [21], Rh@silicalite-1 [22]) have been successively synthesized. However, the potential application of this catalyst in the catalytic oxidation of VOCs is still lacking.

Furthermore, some transition metal promoters have been utilized to regulate noble metals' electronic properties, enhancing their catalytic activity for VOCs [23,24]. Among several transition metals, Mn is widely

* Corresponding authors at: Tianjin Key Lab of Indoor Air Environmental Quality Control, School of Environmental Science and Technology, Tianjin University, Tianjin 300350, China.
E-mail addresses: liuql@tju.edu.cn (Q. Liu), hanr@tju.edu.cn (R. Han).

https://doi.org/10.1016/j.apcatb.2022.121224
Received 27 October 2021; Received in revised form 29 January 2022; Accepted 15 February 2022
Available online 17 February 2022

studied for the VOCs elimination due to its multiple coordination numbers, oxidation states, and high redox potential [25,26]. Zhao et al. [27] demonstrated that introducing Mn into Pd/TiO_2 catalyst increased the content of adsorbed oxygen and improved the low-temperature reducibility. In existing research, most of the bimetal-based active phase is dispersed on the surface of supports, which is easy to agglomerate under harsh conditions. Encapsulating the bimetal-based active phase within the zeolite is expected to improve its activity and stability significantly. However, there are few reports on bimetal@zeolite catalysts because the synthesis process is difficult to control [28].

Herein, ZSM-5 zeolite-confined PtMn bimetal catalysts ($PtMn_x$ @ZSM5) were synthesized by a one-pot hydrothermal method and exhibited extraordinary performance for acetone catalytic oxidation. ZSM-5 zeolite was chosen as the target support due to its good VOC adsorption capacity, excellent hydrophobicity, and thermal stability. During the one-pot hydrothermal process, the critical procedure is introducing organic ligands to prevent metal precursors from aggregation and precipitation under alkaline conditions [29–31]. Through catalytic performance testing and characterization of the samples, we explored the confinement effect of zeolite and the synergistic effect of Pt and Mn. Furthermore, a possible mechanism for acetone oxidation on $PtMn_x$ @ZSM5 was revealed.

2. Experimental

2.1. Materials

All reagents were used without any further purification. Tetrapropylammonium hydroxide solution (TPAOH, 40 wt%) was purchased from Shanghai D&B Biological Science and Technology Co., Ltd. Tetraethylorthosilicate (TEOS) and tetraethylenepentamine (TEPA) were obtained from Tianjin Kermel Chemical Reagent Co., Ltd. Aluminium isopropoxide was bought from Shanghai Macklin Biochemical Co., Ltd. Ethylenediamine (EDA) was purchased from Tianjin Guangfu Technology Development Co., Ltd. $Mn(NO_3)_2$ (50 wt% solution) was obtained from Shanghai Rhawn Reagent Co., Ltd. H_2PtCl_6 was purchased from Tianjin Chemart Chemical Technology Co., Ltd.

2.2. Synthesis of catalysts

2.2.1. Preparation of Pt-EDA and Mn-TEPA precursor solutions

The Pt-EDA solution was prepared by adding 5.37 mL H_2PtCl_6 aqueous solution (19.3 mmol/L) into 4.03 g ethylenediamine (EDA) under stirring until obtaining a clear solution. The Mn-TEPA solution was prepared by dissolving 1.0 g $Mn(NO_3)_2$ aqueous solution (50 wt%) into 9 mL of an aqueous solution containing 1.5 mL of tetraethylenepentamine (TEPA) under stirring until becoming a clear solution. It is worth noting that the Mn-TEPA solution needs to be used immediately after preparation. Otherwise, it will precipitate soon.

2.2.2. Synthesis of Pt@ZSM5

Pt@ZSM5 was prepared according to the research of Sun et al. [32], with some modifications. Typically, 8.14 g TPAOH solution and 0.0544 g aluminum isopropoxide were dissolved into 19 g deionized water. Then the Pt-EDA solution was added to the mixture and stirred for 30 min. After the solution became clear, 8.32 g TEOS was added and stirred continuously for 12 h. The resulting solution was then transferred into a 100 mL Teflon-lined stainless steel autoclave and crystallized in an oven at 170 ℃ for 72 h. After cooling to room temperature, the as-synthesized precipitation was centrifuged, washed several times, and dried at 100 ℃ for 12 h. Finally, the product was calcined at 550 ℃ for 4 h in air.

2.2.3. Synthesis of $PtMn_x$ @ZSM5

$PtMn_x$ @ZSM5 was synthesized with a similar procedure to Pt@ZSM5 except for introducing different amounts of Mn-TEPA precursor solution (0.27, 0.67, 2.68 mL) when adding Pt-EDA solution. According to the different Mn/Pt mass ratios in the final samples, the catalysts were named $PtMn_{0.2}$ @ZSM5, $PtMn_{0.5}$ @ZSM5, $PtMn_1$ @ZSM5, respectively (x refers to the Mn/Pt mass ratio).

In addition, the detailed synthesis of $Mn_{0.2}$ @ZSM5, ZSM-5, Pt/ZSM5, $PtMn_{0.2}$/ZSM5, $Mn_{0.2}$/Pt@ZSM5 was shown in the Supplementary Information. Notably, all the catalysts were used directly after the calcination, without any reduction treatment. The procedures of these catalysts are shown in Fig. 1.

2.3. Catalysts characterization

The catalysts were characterized by X-ray diffraction (XRD), high-resolution transmission electron microscope (HRTEM), inductively coupled plasma atomic emission spectrometry (ICP-AES), N_2 adsorption-desorption, H_2 chemisorption, NH_3 temperature-programmed desorption (NH_3-TPD), O_2 temperature-programmed desorption (O_2-TPD), H_2 temperature-programmed reduction (H_2-TPR), X-ray photoelectron spectroscopy (XPS), Pyridine adsorption Fourier-transform infrared (pyridine FT-IR), Acetone temperature-programmed desorption (Acetone-TPD), and In-situ DRIFTS. The detailed characterization procedures were described in Supplementary Information.

2.4. Catalytic activity tests

The catalytic oxidation tests of acetone were carried out in a fix-bed quartz tube (8 mm i.d. × 400 mm length), and a certain amount of samples (40–60 mesh) were placed in the middle of it. When acetone-mixed gas flowed through the quartz tube, it was oxidized by the fixed catalysts under a temperature-programmed condition controlled by an electric furnace. The detailed procedures and conditions of tests were shown in the Supplementary Information.

The concentration of acetone and CO_2 were monitored online by a gas chromatograph (GC-9790II FuLi) with two FID detectors. Specifically, the acetone was analyzed by one FID detector, and the CO_2 was analyzed by the other FID detector equipped with a reformer. The acetone conversion (X) and CO_2 yield (Y) were calculated as follows:

$$X = ([acetone]_{in} - [acetone]_{out}) / [acetone]_{in} \times 100\% \quad (1)$$

$$Y = ([CO_2] / [CO_2^*]) \times 100\% \quad (2)$$

where $[acetone]_{in}$ and $[acetone]_{out}$ are the acetone concentrations before and after the reaction, respectively. $[CO_2^*]$ is the CO_2 concentration after acetone was oxidized entirely, and $[CO_2]$ is the CO_2 concentration at various temperature points.

The calculations of activation energy and turnover frequency (TOF) are shown in the Supplementary Information.

3. Results and discussion

3.1. Physical properties

The zeolite-confined catalysts' actual and theoretical metal loads are shown in Tables 1 and S1. The actual metal loads were slightly lower than the theoretical loadings, indicating that the Pt and Mn species can not be fully loaded into ZSM-5 during the hydrothermal process.

XRD patterns of the catalysts are shown in Figs. 2a and S2. The obtained catalysts presented well-defined diffraction peaks ascribed to the ZSM-5 crystalline structure. No distinct characteristic peaks related to Pt or Mn species were detected because of the low metal loading and high dispersion. The samples obtained by the in-situ synthesis method exhibited equivalent peak intensity as the pure ZSM-5 support, which demonstrated that the addition of metal precursors in synthetic gel had little effect on the crystallization of the ZSM-5 zeolite.

N_2 adsorption-desorption isotherms and pore size distribution curves are presented in Figs. 2b-d and S3. These catalysts exhibited typical

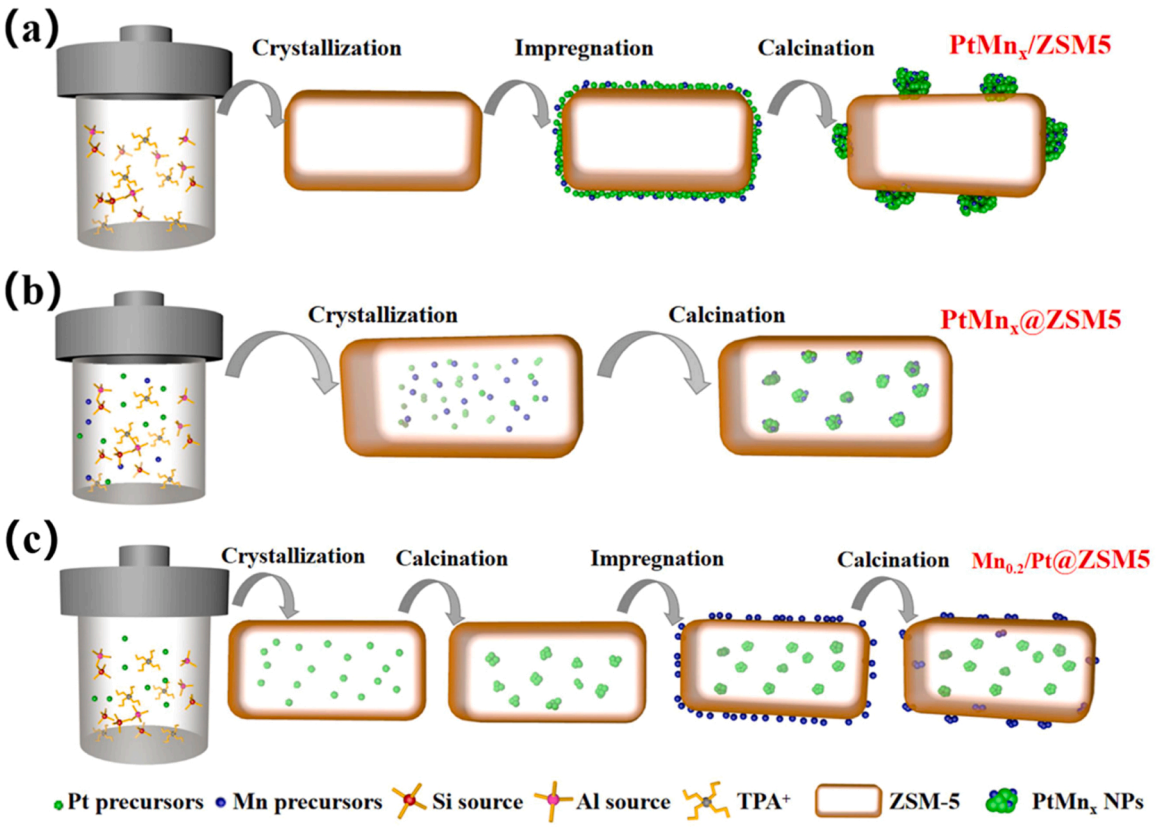

Fig. 1. Schematic illustration of the synthetic procedure of (a) $PtMn_x$/ZSM5, (b) $PtMn_x$ @ZSM5 and (c) $Mn_{0.2}$/Pt@ZSM5 catalysts.

Table 1
Physical properties and chemical composition of the catalysts.

Catalyst	S_{BET}[a] (m^2/g)	V_{Pore}[b] (cm^3/g)	Pt loading[c] (wt%)	Mn loading[c] (wt%)	Pt dispersion[d] (%)	SiO_2/Al_2O_3[c]
ZSM-5	393.2	0.25	/	/	/	243.6
Pt@ZSM5	375.1	0.20	0.66	/	12.53	262.0
$PtMn_{0.2}$ @ZSM5	327.8	0.18	0.66	0.14	4.50	245.6
$PtMn_{0.5}$ @ZSM5	367.3	0.20	0.65	0.27	2.60	274.0
$PtMn_1$ @ZSM5	314.5	0.17	0.60	0.61	6.73	279.6
Pt/ZSM5	322.5	0.18	0.65	/	0.55	266.4
$PtMn_{0.2}$/ZSM5	354.9	0.20	0.62	0.19	0.25	278.8
$Mn_{0.2}$ @ZSM5	/	/	/	0.16	/	243.6
$Mn_{0.2}$/Pt@ZSM5	/	/	0.67	0.22	6.20	263.2

[a] Surface area by Brunauer-Emmett-Teller (BET) method.
[b] Total pore volumes of $P / P^0 = 0.95$.
[c] Determined by ICP-AES analysis.
[d] Determined by H_2 chemisorption. The detailed calculation was shown in the Supplementary Information.

isotherms of type-I, which indicated the presence of microporosity, and their pore sizes were mainly distributed in 0.5–2.0 nm. The physical parameters of these catalysts are shown in Table 1. They all possessed a high surface area (> 300 m^2/g) which can provide abundant sites for the adsorption of acetone and oxygen molecules. Compared with the pure ZSM-5, the metal-loaded catalysts showed a relatively lower specific surface area and pore volume, which may be related to the blocking of pores by metal nanoparticles. The Pt dispersion in Pt@ZSM5 was the highest (12.53%), and it decreased to 4.50% and 2.60% in $PtMn_{0.2}$ @ZSM5 and $PtMn_{0.5}$ @ZSM5, respectively. However, as the content of Mn further increased, the Pt dispersion of $PtMn_1$ @ZSM5 rebounded to 6.73%. The initial decrease of Pt dispersion was possible due to the partial cover of MnO_x species on the Pt surface. However, much higher Mn content tended to form the preferential self-aggregation of MnO_x and weakened the Pt-Mn interaction, thus resulting in the rebound of Pt dispersion [33]. As for the samples prepared by the impregnation method, the Pt/ZSM5 and $PtMn_{0.2}$/ZSM5 showed much lower Pt dispersion (< 1%), suggesting the severe aggregation of Pt.

3.2. Morphology characteristics

According to the HRTEM images of the catalysts (Figs. 3 and S4), the metal nanoparticles were successfully confined in zeolite crystals through the in-situ synthesis method. In contrast, the metal nanoparticles were unevenly loaded on the outer surface of zeolite through the conventional impregnation method.

Significantly, the well-dispersed Pt nanoparticles in Pt@ZSM5 exhibited an average size of 4.68 nm, much smaller than that of Pt/ZSM5 (12.16 nm) (Fig. S4a-c). Notably, because the metal sizes were much larger than the micropores of ZSM-5 (around 0.55 nm), these metal species were fixed by the zeolite framework rather than encapsulated in the zeolite's pores. When a little Mn (0.14 wt%) was

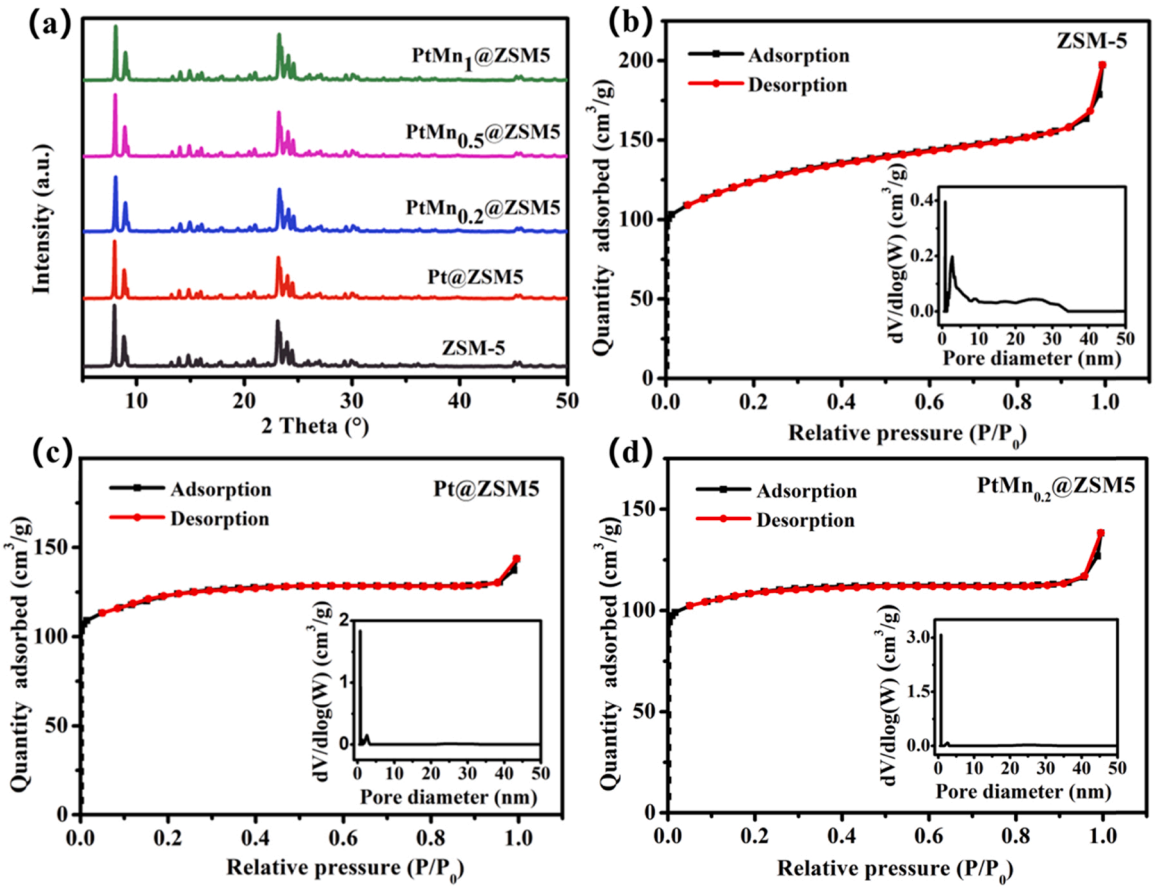

Fig. 2. (a) The XRD patterns of ZSM-5, Pt@ZSM5, $PtMn_{0.2}$ @ZSM5, $PtMn_{0.5}$ @ZSM5, and $PtMn_1$ @ZSM5 catalysts. The N_2 adsorption-desorption curve and pore diameter distribution of (b) ZSM-5, (c) Pt@ZSM5, (d) $PtMn_{0.2}$ @ZSM5.

introduced into Pt@ZSM5, most of the resulting bimetal nanoparticles remained confined structure (Fig. 3a-b). Compared with Pt@ZSM5, $PtMn_{0.2}$ @ZSM5 showed a larger average size of 6.42 nm. It was probably because the incorporated Mn^{2+} species with positive charge showed attractive force to the negative ligand-complexed $[PtCl_6]^{2-}$ species during the crystallization process [33]. After the subsequent calcination process, the resulting MnO_x partially covered the Pt nanoparticles to form larger metal nanoparticles than that in Pt@ZSM5. Despite that, the metal nanoparticles of $PtMn_{0.2}$ @ZSM5 still showed much smaller size than that of $PtMn_{0.2}$/ZSM5 (15.08 nm) (Fig. 3d), which demonstrated that the rigid zeolite framework effectively stabilized the confined metal species during the high-temperature calcination process. When the Mn was loaded on the Pt@ZSM5 by the post impregnation, the average size of Pt nanoparticles in $Mn_{0.2}$/Pt@ZSM5 (4.90 nm) was similar to that in Pt@ZSM5 (Fig. S4g) due to lack the interaction between Pt and Mn. The interplanar distances of these catalysts were 0.23 nm, corresponding to the typical (111) plane of Pt (Fig. 3c, f) [8], and no lattice fringes related to Mn species were observed because of its lower content. From the EDS-mapping images (Fig. 3g-j), the uniform distribution of Pt and Mn in $PtMn_{0.2}$ @ZSM5 was confirmed, which was beneficial to enhance their interaction effect.

3.3. Catalytic activity

The catalytic activity of the samples was investigated under the feed gas containing 5 vol% water vapor (Fig. 4). The pure ZSM-5 support had poor activity on acetone oxidation, and the metal-encapsulated catalysts exhibited better performance than the metal-supported catalysts (Fig. 4a). Notably, the introduction of Mn into Pt@ZSM5 significantly promoted the conversion of acetone at low temperatures, even at a low loading (0.14 wt%). Considering the weak activity exhibited by independent Mn species, it can be speculated that the promotion of acetone oxidation is attributed to a synergy effect between Pt and Mn, resulting from the interaction and modulation of their electronic structure [34]. The $PtMn_{0.2}$ @ZSM5 catalyst showed the best performance in all samples with a T_{95} of 165 ℃. Compared to the previously reported noble metal-based catalysts, the $PtMn_{0.2}$ @ZSM5 in this work showed great superiority in the catalytic activity for acetone oxidation (Table S2).

To further verify the synergy effect between Pt and Mn, the $Mn_{0.2}$/Pt@ZSM5 was designed by a two-step synthesis to separate Pt and Mn, thus limiting the electron transfer between Pt and Mn. As a result, the $Mn_{0.2}$/Pt@ZSM5 showed lower catalytic activity than $PtMn_{0.2}$/ZSM5 and $PtMn_{0.2}$ @ZSM5 for lack of the bimetallic interaction, which confirmed the significance of PtMn bimetal synergy effect for high catalytic efficiency.

The CO_2 yields of these catalysts (Fig. 4b) were relatively lower than their corresponding acetone conversions at the lower temperature, suggesting the presence of some incompletely oxidized by-products. However, no other products were detected except for CO_2. The by-products may be adsorbed on the ZSM-5 catalysts owing to their large specific surface area and abundant acid sites. When the temperature increased to 180 ℃, the CO_2 yield increased to 97%, nearly matching the corresponding acetone conversion (99%), which demonstrated the complete oxidation of acetone. Fig. 4c showed the catalytic activity of the $PtMn_{0.2}$ @ZSM5 catalyst under dry and wet (5 vol% water) gas conditions. The introduction of water vapor into the system had little effect on the acetone conversion. This excellent water resistance of the $PtMn_{0.2}$ @ZSM5 was attributed to its high SiO_2/Al_2O_3 ratio (> 240), which enhanced the hydrophobicity of zeolite and weakened the competitive adsorption of water.

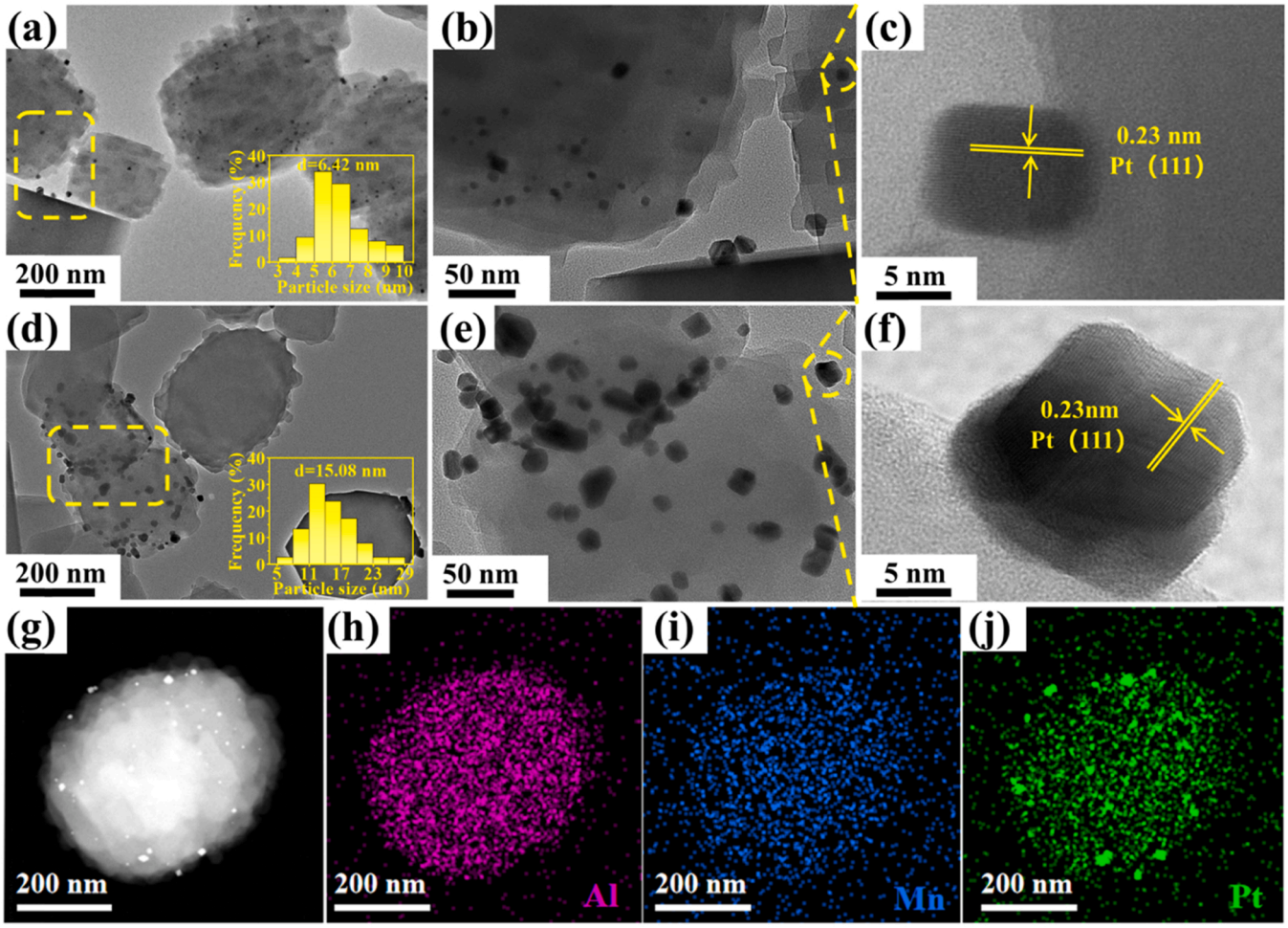

Fig. 3. HRTEM of (a-c) $PtMn_{0.2}$ @ZSM5, (d-f) $PtMn_{0.2}$/ZSM5. (g) TEM image of $PtMn_{0.2}$ @ZSM5, and EDS elemental maps of (h) Al, (i) Mn, and (j) Pt, respectively.

The kinetics study was performed to investigate the activation energy of the catalysts, which closely affected the reaction rate. As shown in Fig. 4d, the sequence of E_a followed the order of Pt/ZSM5 (87.5 kJ·mol^{-1}) > Pt@ZSM5 (79.5 kJ·mol^{-1}) > $Mn_{0.2}$/Pt@ZSM5 (60.4 kJ·mol^{-1}) > $PtMn_{0.2}$/ZSM5 (45.6 kJ·mol^{-1}) > $PtMn_{0.2}$ @ZSM5 (42.3 kJ·mol^{-1}), which was in line with their catalytic activity. The lowest E_a value of the $PtMn_{0.2}$ @ZSM5 confirmed its superior activation properties in acetone oxidation.

The different $PtMn_x$ @ZSM5 catalysts were tested to evaluate the effect of Mn/Pt mass ratios on acetone oxidation. As shown in Fig. 5a, the catalytic activity of $PtMn_{0.2}$ @ZSM5 and $PtMn_{0.5}$ @ZSM5 was equivalent, indicating that the increase of Mn loading has no further promotion effect. On the contrary, when the Mn/Pt mass ratio increased to 1, the corresponding $PtMn_1$ @ZSM5 catalyst exhibited a lower acetone conversion. An Mn/Pt mass ratio of 0.2 seems to result in a proper Pt-Mn interaction. In addition, The CO_2 yield curves (Fig. 5b) indicated the deep oxidation of acetone over these catalysts.

Based on the Pt dispersion measured by the H_2 chemisorption, turnover frequency (TOF) of different $PtMn_x$ @ZSM5 catalysts was calculated, and its order was as follows: $PtMn_{0.2}$ @ZSM5 (4.66×10^{-2} s^{-1}) > $PtMn_{0.5}$ @ZSM5 (3.92×10^{-2} s^{-1}) > $PtMn_1$ @ZSM5 (1.16×10^{-2} s^{-1}) > Pt@ZSM5 (2.83×10^{-3} s^{-1}) (Fig. 5c). Significantly, such TOF value was a combined contribution of both bare Pt atoms and Pt-Mn interfacial sites, so it is necessary to investigate the respective effects of these two sites. Inspired by the literature [35], the TOF of bare Pt atoms (TOF_{Pt}, 2.83×10^{-3} s^{-1}) was easily obtained by Pt@ZSM5 without any Mn species, which was assumed to be a setting value in the different $PtMn_x$ @ZSM5 catalysts. Then, the TOF of Pt-Mn interfacial sites was calculated by the following equation: TOF_{Pt} × quantity of Pt sites + $TOF_{Pt\text{-}Mn}$ × quantity of Pt-Mn sites = overall reaction rate, in which the quantity of Pt-Mn interfacial sites was still waiting to be resolved.

Although the HRTEM results showed a larger Pt nanoparticles size in PtMnx@ZSM5 than that in Pt@ZSM5, we tended to believe that it was due to Mn species' coverage. Suppose the Pt particle sizes in all catalysts are the same. In that case, the theoretical quantity of surface Pt sites could be obtained by the actual Pt content in different $PtMn_x$ @ZSM5 catalysts. However, the actual measured quantity of Pt sites was undoubtedly lower than the theoretical value because of the coverage of Mn, so we considered this difference value as the quantity of Pt-Mn interfacial sites. Despite the possible error in the calculation, it could still provide valuable information.

The detailed calculation and results are summarized in Table 2 (the calculation process shown in Supplementary Information). It showed that the Pt-Mn interfacial sites showed much higher activity (TOF) than the bare Pt surface atoms, which was responsible for the better overall activity of $PtMn_x$ @ZSM5 than Pt@ZSM5. Significantly, the $TOF_{Pt\text{-}Mn}$ of $PtMn_{0.2}$ @ZSM5 reached 2.45×10^{-2} s^{-1}, more than twice of $PtMn_{0.5}$ @ZSM5 and $PtMn_1$ @ZSM5 (Fig. 5d), which corresponded to its best catalytic activity. These results suggested that the proper Pt-Mn interaction played a crucial role in enhancing catalytic activity and the Pt-Mn interfacial sites acted as the main active sites.

3.4. XPS

The XPS characterization for the Pt@ZSM5 and $PtMn_{0.2}$ @ZSM5 was carried out to verify the interaction between Pt and Mn. As shown in

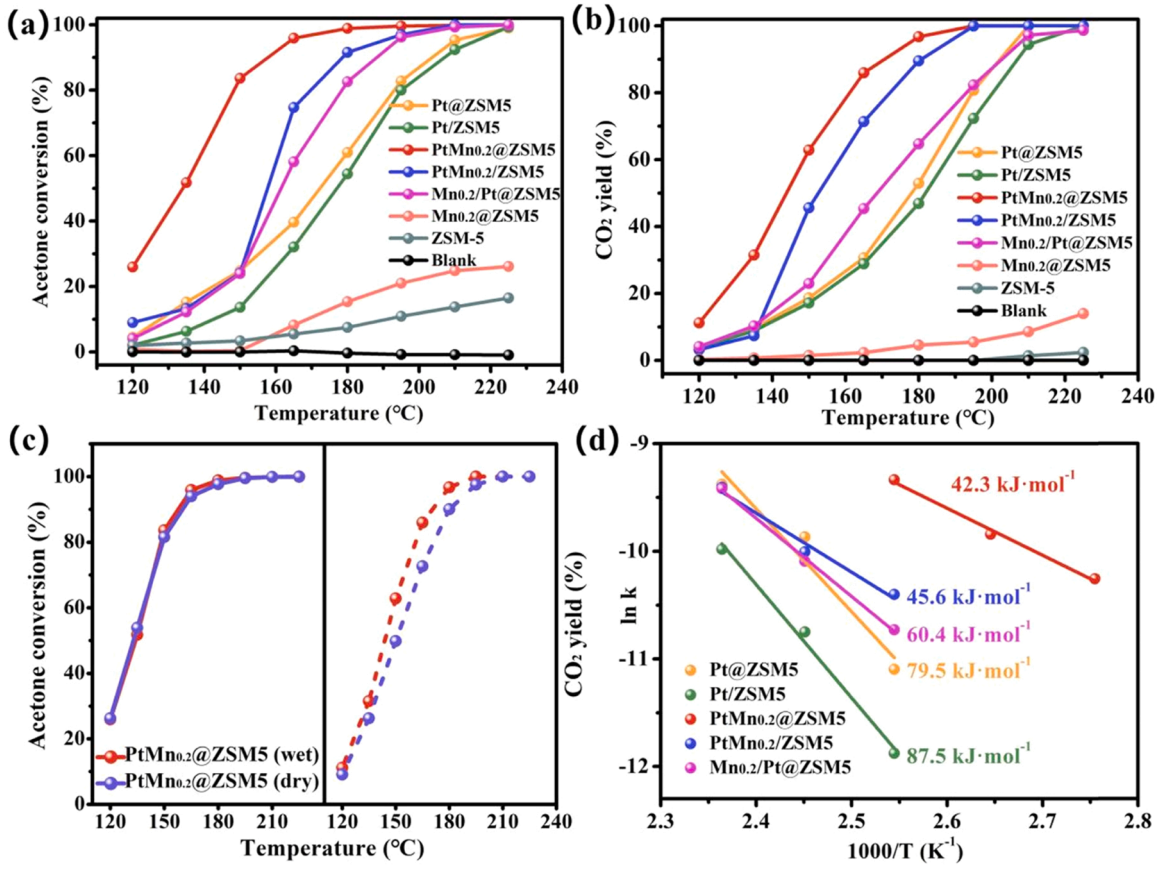

Fig. 4. (a) Acetone conversion and (b) CO_2 yield over these catalysts under 5% water vapor condition. (c) Catalytic activity of the $PtMn_{0.2}$ @ZSM5 catalyst under wet and dry gas conditions. (d) Arrhenius plots of the catalysts under 5% water vapor condition.

Fig. 6a, in the Pt 4 f XPS spectra, the components at the Binding energy of about 71.2 eV, 72.1 eV, and 74.5 eV were assigned to the Pt^0, Pt^{2+}, and Pt^{4+} species, respectively [11,23]. The ratios of $Pt^0/Pt^0+Pt^{2+}+Pt^{4+}$ were estimated and listed in Table S3. Compared with Pt@ZSM5 (35.7%), $PtMn_{0.2}$ @ZSM5 possessed a higher ratio of Pt^0 (44.0%). The higher Pt^0 species of $PtMn_{0.2}$ @ZSM5 is probably attributed to the electron transfer from Mn to Pt. Generally, the reduced Pt^0 species were more active than deeply oxidized Pt ions in VOCs catalytic oxidation. Jeong [36] et al. found that the increase of Pt^0 ratio from 16.6% to 83.8% significantly improved the catalytic activity for CH_4 combustion. Chen [37] et al. proposed that the Pt atoms at a low-coordination environment could accelerate oxygen mobility, leading to a remarkable catalytic activity for HCHO oxidation. Therefore, the increase of Pt^0 was beneficial to enhancing catalytic activity. Owing to Mn's ultra-low content, there were no signal peaks in the Mn 2p XPS spectra (Fig. 6b).

3.5. NH_3-TPD and pyridine FT-IR

The acidity of the catalysts is a crucial factor for catalytic activity, which can directly affect the adsorption of VOC molecules [38]. To detect the acidic properties, NH_3-TPD was carried out, and the profiles are shown in Fig. 7a. There were mainly two desorption peaks in the temperature ranges of 100–120 ℃ and 300–400 ℃, which were related to the weak acid and strong acid sites, respectively [39]. The quantitative desorption results are presented in Table S4. Compared with the ZSM-5 support, the Pt@ZSM5 and $Mn_{0.2}$/Pt@ZSM5 catalysts possessed a similar content of both acid sites, while the $PtMn_{0.2}$/ZSM5 presented lower weak acid sites. The decrease of weak acid sites was probably because the larger metal nanoparticles occupied the weak acid sites on the surface of ZSM-5 support [40]. Significantly, thanks to the combination of zeolite confinement and PtMn synergy, the $PtMn_{0.2}$ @ZSM5 achieved the highest levels of both weak and strong acid sites. These abundant acid sites enhanced the adsorption of acetone and strengthened the interaction between reactant and active phase [41]. Besides, more strong acid sites were beneficial to desorb the acidic product CO_2, which could further accelerate the reaction proceeding [42].

It is generally recognized that the NH_3 adsorbed on Lewis acid sites is more thermally stable than that adsorbed on Brønsted acid sites during the TPD process [43]. Therefore, the enhanced strong acid sites by PtMn bimetal interaction in $PtMn_{0.2}$ @ZSM5 may belong to the Lewis acid sites. The pyridine FT-IR of the Pt@ZSM5 and $PtMn_{0.2}$ @ZSM5 was performed to confirm the assumption. As shown in Fig. 7b, the $PtMn_{0.2}$ @ZSM5 showed a higher characteristic peak at 1450 cm^{-1} assigned to the L-acid sites, while the B-acid sites of both catalysts were equivalent (Table S5). It demonstrated that the PtMn interaction mainly enhanced the Lewis acidity due to the electron transfer from Mn to Pt [33], consistent with XPS results. This electron transfer leads to more Mn ions with high electron-accepting ability, increasing Lewis acid centers. Notably, it has been reported that the Lewis acid sites were important active sites for C-C band cleavage. Hence the $PtMn_{0.2}$ @ZSM5 with high Lewis acidity exhibited excellent catalytic performance [44].

3.6. Acetone-TPD

Acetone-TPD experiment was performed to verify the enhanced acetone adsorption over $PtMn_{0.2}$ @ZSM5, which generated more acid sites by the PtMn interaction. As shown in Fig. 8a, the outlet acetone concentration decreased rapidly when the acetone feed gas flowed into the catalyst fixed bed, attributed to the large surface area and strong adsorption of the samples. Notably, the penetration time of $PtMn_{0.2}$ @ZSM5 was longer than that of Pt@ZSM5, suggesting its higher acetone adsorption capacity. When acetone gas was cut off and purging with N_2,

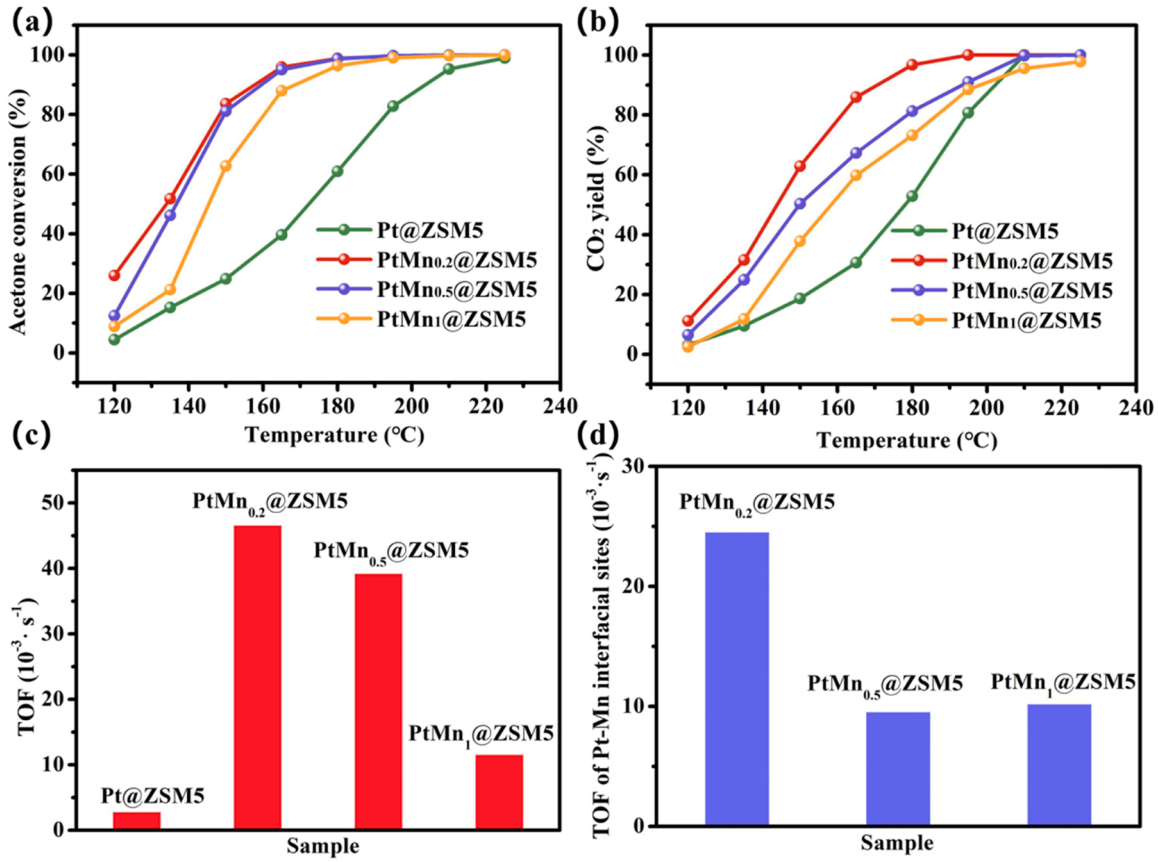

Fig. 5. (a) Acetone conversion and (b) CO_2 yield over different $PtMn_x$ @ZSM5 catalysts. (c) TOF values of the catalysts based on the actual Pt content, Pt dispersion, and the reaction rate at 120 ℃. (d) TOF of Pt-Mn interfacial sites based on the following equation: $TOF_{Pt} \times$ quantity of Pt sites + $TOF_{Pt\text{-}Mn} \times$ quantity of Pt-Mn sites = overall reaction rate.

Table 2
Estimation of the quantity of Pt-Mn interfacial sites and their TOFs in the different $PtMn_x$ @ZSM5 catalysts.

Catalyst	Theoretical quantity of surface Pt sites[a] ($\mu mol^{-1}g_{cat}^{-1}$)	Actual quantity of surface Pt sites[b] ($\mu mol^{-1}g_{cat}^{-1}$)	TOF of surface Pt sites[c] ($10^{-3}\cdot s^{-1}$)	Quantity of Pt-Mn interfacial sites[d] ($\mu mol^{-1}g_{cat}^{-1}$)	Reaction rate ($\mu mol^{-1}g_{cat}^{-1}s^{-1}$)	TOF of Pt-Mn interfacial sites[e] ($10^{-3}\cdot s^{-1}$)
Pt@ZSM5	4.24	4.24	2.83	/	0.012	/
$PtMn_{0.2}$ @ZSM5	4.24	1.52	2.83	2.72	0.071	24.52
$PtMn_{0.5}$ @ZSM5	4.18	0.87	2.83	3.31	0.034	9.53
$PtMn_1$ @ZSM5	3.85	2.07	2.83	1.78	0.024	10.19

[a] Assuming that the Pt particle sizes in all the catalysts were the same, and the theoretical quantity of surface Pt sites was calculated based on the actual Pt contents.
[b] Actual quantity of surface Pt sites obtained by H_2 chemisorption.
[c] Assuming that the assessable surface Pt sites in all the catalysts possessed the same catalytic activity, that is, the TOF value of Pt@ZSM5.
[d] Quantity of the surface Pt-Mn interfacial sites = Theoretical quantity of surface Pt sites - Actual quantity of surface Pt sites.
[e] TOF of Pt-Mn interfacial sites was calculated following equation: $TOF_{Pt} \times$ quantity of Pt sites + $TOF_{Pt\text{-}Mn} \times$ quantity of Pt-Mn sites = reaction rate.

the physically adsorbed acetone on both catalysts was desorbed simultaneously. Fig. 8b showed the temperature-programmed desorption profile of acetone. The acetone was mainly desorbed between 120 ℃ and 200 ℃, and also, the $PtMn_{0.2}$ @ZSM5 presented more adsorption content of acetone than Pt@ZSM5 even the former had a lower specific surface area (Table 1). These results of acetone-TPD confirmed that the $PtMn_{0.2}$ @ZSM5 showed better acetone adsorption performance than Pt@ZSM5 owing to the more acid sites generated by PtMn interaction.

3.7. O_2-TPD and H_2-TPR

O_2-TPD experiments were conducted to investigate the evolution of oxygen species. According to different temperature regions of oxygen desorption, these desorbed oxygen species can be divided into three types [45]: surface adsorbed oxygen (O_{ads}, < 200 ℃), surface lattice oxygen ($O_{s\text{-}latt}$, 200–600 ℃) and bulk lattice oxygen ($O_{b\text{-}latt}$, > 600 ℃) (Fig. 9a). O_{ads} species (e.g., O_2^- and O^-) are the most active and play a crucial role in the oxidation of VOCs [46]. The $Mn_{0.2}$/Pt@ZSM5 showed an equivalent O_{ads} content with Pt@ZSM5, while $PtMn_{0.2}$ @ZSM5 was much more than them (Table 3). It strongly demonstrated that the direct electron transfers from Mn to Pt significantly improved the O_{ads} content. The metallic Pt^0 was generally easier to transfer electrons to gaseous oxygen, which enhanced the adsorption and activation of oxygen[47, 48]. Besides, the metal particle size significantly influenced the catalytic

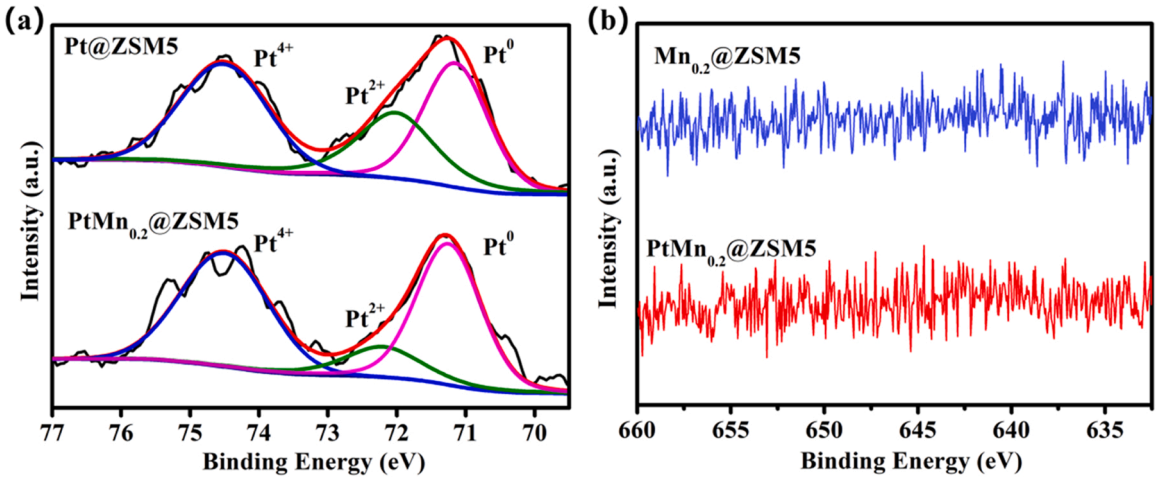

Fig. 6. (a) Pt 4 f XPS spectra of Pt@ZSM5 and $PtMn_{0.2}$ @ZSM5. (b) Mn 2p XPS spectra of $Mn_{0.2}$ @ZSM5 and $PtMn_{0.2}$ @ZSM5.

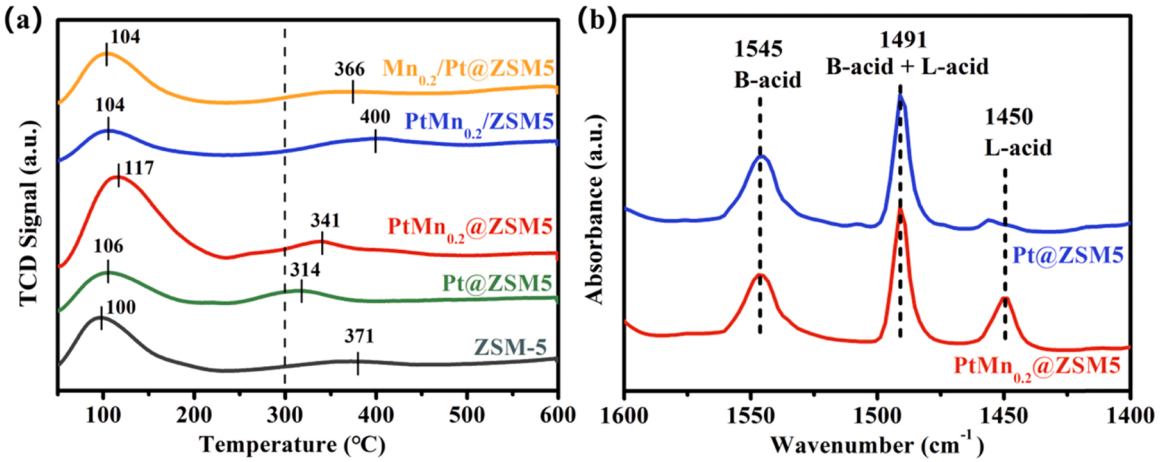

Fig. 7. (a) NH_3-TPD profiles of the samples. (b) Pyridine FT-IR profiles of the Pt@ZSM5 and $PtMn_{0.2}$ @ZSM5.

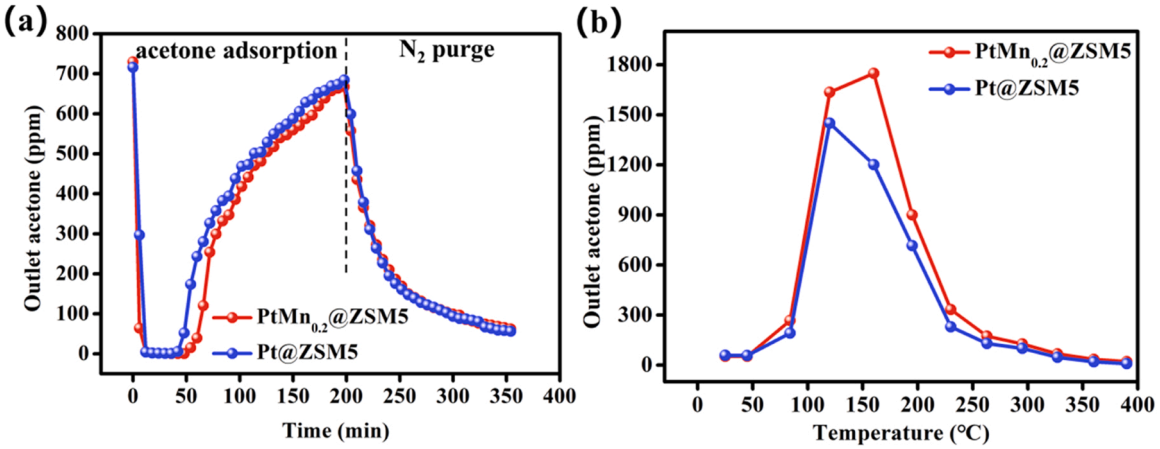

Fig. 8. (a) Acetone adsorption and N_2 purge process at room temperature. (b) Acetone temperature-programmed desorption process.

dissociation of O_2. Owing to the larger particle size and limited exposed active sites, the $PtMn_{0.2}$/ZSM5 presented the lowest O_{ads} content. Nevertheless, the $PtMn_{0.2}$/ZSM5 exhibited the most $O_{s\text{-}latt}$, and its desorption temperature (237 ℃, 338 ℃) was much lower than that of the $PtMn_{0.2}$ @ZSM5 (504 ℃). The decrease of desorption temperature indicated the enhanced mobility of lattice oxygen, which was probably attributed to the bulk surface Mn oxides. The oxygen desorption peaks of the $Mn_{0.2}$/Pt@ZSM5 were close to that of the $PtMn_{0.2}$/ZSM5, but the desorption content was the least. $O_{b\text{-}latt}$ is generally considered not a contributing factor for reaction in the lower temperature due to its high migration resistance. Overall, the catalytic activity was the combined result of O_{ads} and $O_{s\text{-}latt}$. Thanks to the zeolitic confinement and PtMn

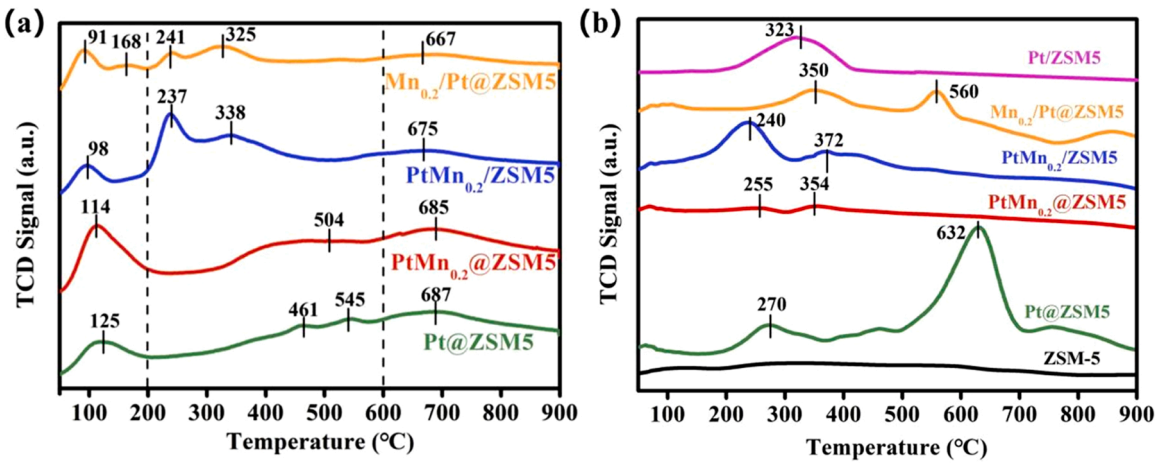

Fig. 9. (a) O_2-TPD profiles and (b) H_2-TPR profiles of different samples.

Table 3
Oxygen species of the catalysts.

Catalyst	O_{ads} (mmol/g)	$O_{s\text{-}latt}$ (mmol/g)	$O_{b\text{-}latt}$ (mmol/g)
Pt@ZSM5	0.29	1.08	1.44
$PtMn_{0.2}$ @ZSM5	0.56	1.00	1.37
$PtMn_{0.2}$/ZSM5	0.11	1.24	1.13
$Mn_{0.2}$/Pt@ZSM5	0.27	0.67	0.81

bimetal interaction, the $PtMn_{0.2}$ @ZSM5 exhibited the most abundant active oxygen species, responsible for its outstanding catalytic activity.

Fig. 9b showed the H_2-TPR curves of these catalysts, which were helpful to understanding the roles of metals in the composite materials. There were no obvious peaks in the pure ZSM-5 support, suggesting it had no reducibility. The peaks at 240–323 ℃ and 350–372 ℃ were attributed to the reduction of PtO_x [11] and MnO_x [26], respectively, while the peaks at 560–632 ℃ could be assigned to the Pt species coordinated with silanol sites within zeolite [49], indicating the strong

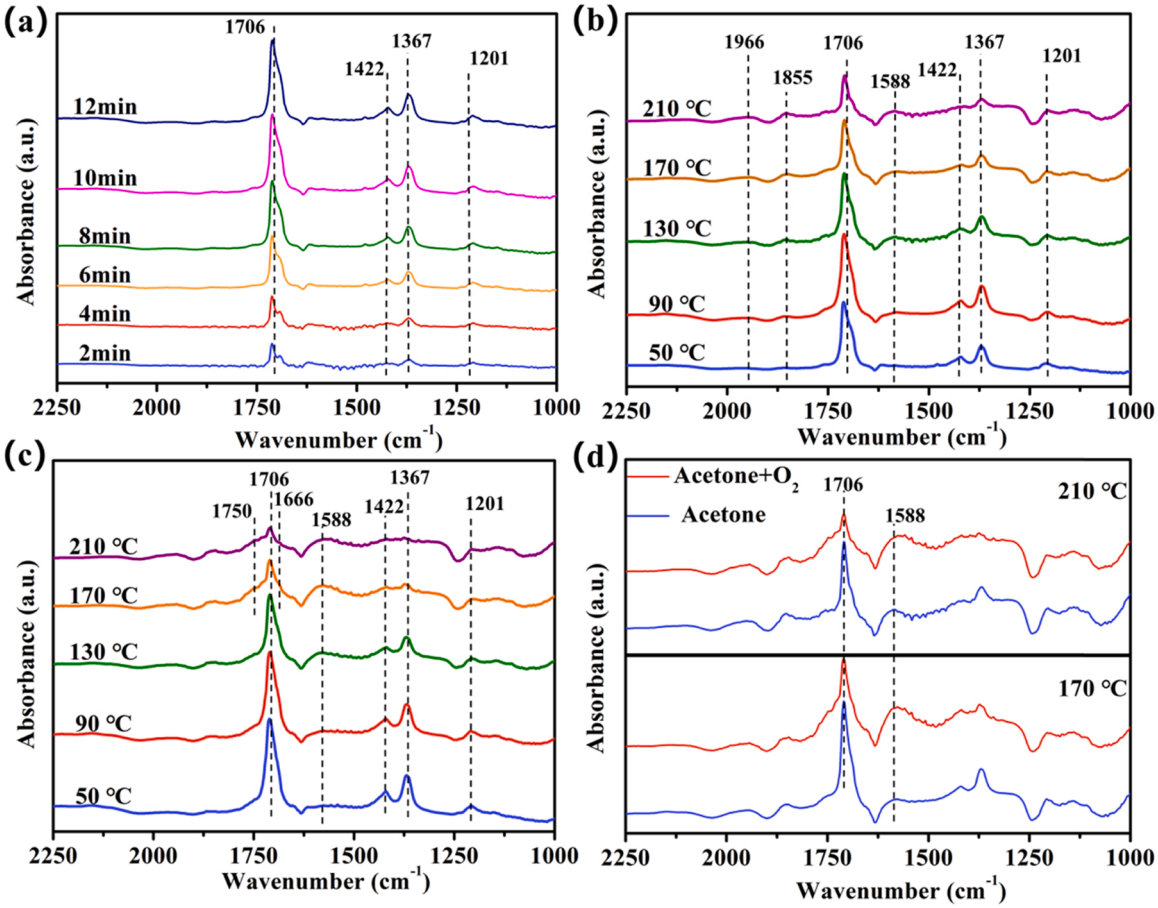

Fig. 10. (a) In-situ DRIFTS spectra of acetone adsorption over $PtMn_{0.2}$ @ZSM5 at 50 ℃ at different times. In-situ DRIFTS spectra of acetone catalytic oxidation over the $PtMn_{0.2}$ @ZSM5 at different temperatures (b) in the absence of gas-phase oxygen and (c) in the presence of gas-phase oxygen, and (d) the comparison under these two conditions.

interaction between confined Pt species and zeolite frameworks. However, this high-temperature peak was not observed in the Pt/ZSM5 and $PtMn_{0.2}$/ZSM5, suggesting that the supported Pt species were mainly PtO_x, much different from the confined ones owing to the different Pt-zeolite interaction. Interestingly, When Mn was incorporated into Pt@ZSM5 catalyst, the reduction peaks corresponding to Pt species had significantly decreased, which confirmed the reduction of Pt ions by the addition of Mn. The above analysis is consistent with the XPS results (Fig. 6a), which confirmed that the metallic Pt^0 species played an essential role in the superior catalytic activity of $PtMn_{0.2}$ @ZSM5.

3.8. Mechanism for the oxidation of acetone over $PtMn_{0.2}$ @ZSM5

In-situ DRIFTS studies were further performed to investigate the generation of products and get an insight into the mechanism of the catalytic oxidation of acetone over the $PtMn_{0.2}$ @ZSM5 catalyst. Firstly, The acetone adsorption process at 50 ℃ was carried out, and the result is shown in Fig. 10a. The bands at 1706, 1422, 1367, and 1207 cm-1 could be assigned to the ν(C═O), $\delta_{as}(CH_3)$, $\delta_s(CH_3)$, and ν(C-C) of adsorbed acetone molecules, respectively [50]. All these characteristic peaks increased rapidly in a short time, approaching adsorption saturation within 12 min, which indicated that acetone molecules could be readily adsorbed on the $PtMn_{0.2}$ @ZSM5 catalyst, which was beneficial to subsequent oxidation redox reaction. Then, the catalytic oxidation of acetone was explored at different temperatures in the absence of gas-phase oxygen (Fig. 10b). As the temperature increased, the peaks corresponding to ν(C═O) (1706 cm^{-1}), $\delta_{as}(CH_3)$ (1422 cm^{-1}), and $\delta_s(CH_3)$ (1367 cm^{-1}) gradually decreased owing to the desorption of acetone. Besides, there are some new peaks appeared. The peak at 1855 cm^{-1} corresponded to the C═O stretching vibration of acetic anhydride, and the peak at 1966 cm^{-1} belonged to linear CO adsorbed on Pt [8], suggesting the partial oxidation of acetone. Moreover, the new peak at 1588 cm^{-1} was the $\nu_{as}(CO_3)$ peak of bidentate carbonate [51], which was derived from the adsorption of CO_2 and reflected the complete oxidation of acetone. Its lower peak intensity demonstrated that the deep oxidation efficiency of acetone was poor in the absence of oxygen.

When the gas-phase O_2 was introduced into the system, the results of DRIFTS spectra are shown in Fig. 10c. The characteristic peaks of acetone (1706, 1422, 1367 cm^{-1}) decreased rapidly with the temperature increasing. At 170 °C and 210 °C, the characteristic peaks of acetone in the O_2-presence condition were much lower than those in the O_2-absence condition (Fig. 10d). Moreover, the CO_2 adsorption peak (1588 cm^{-1}) was increased in the presence of O_2, suggesting that O_2 promoted the complete oxidation of acetone over $PtMn_{0.2}$ @ZSM5. The enhanced oxidation of acetone was due to the generation of sufficient active oxygen species by activating gas-phase O_2. Hence, it can be speculated that the catalytic oxidation of acetone over $PtMn_{0.2}$ @ZSM5 followed the L-H mechanism. In addition, it was notable that two peaks at 1750 and 1666 cm^{-1} appeared at the higher temperature in the O_2-presence condition, which could be attributed to aliphatic carboxylate species and adsorbed H_2O species [8,50], further demonstrating the deep oxidation of acetone.

To conclude, owing to the confinement effect of zeolite and the appropriate PtMn bimetal synergy effect, the $PtMn_{0.2}$ @ZSM5 exhibited the best catalytic performance (Fig. 11a-c). Based on the results of NH_3-TPD, pyridine FT-IR, XPS, O_2-TPD, H_2-TPR, and In-situ DRIFTS characterizations, a possible catalytic L-H mechanism for the oxidation of acetone over $PtMn_{0.2}$ @ZSM5 was proposed, and the reaction pathway is shown in Fig. 11d. Acetone was initially adsorbed on the $PtMn_{0.2}$ @ZSM5 catalyst, the enhanced acidity of which tended to promote the adsorption process and strengthen the interaction between acetone and the active phase. Then the adsorbed acetone underwent a series of redox reactions with the abundant active oxygen species and finally oxidized into harmless CO_2 and H_2O. Significantly, the $PtMn_{0.2}$ @ZSM5 exhibited a higher active Pt^0 content owing to the PtMn interaction, thus enhancing the oxygen-activation ability. The reacted active oxygen species could be quickly replenished by gas-phase oxygen, and further accelerated the degradation of acetone. Finally, the H_2O and CO_2 were desorbed from the catalyst, and its strong acidity was conductive to this desorption process, which was beneficial to the reaction proceeding.

3.9. Durability and applicability of $PtMn_{0.2}$ @ZSM5

The durability of catalysts is one of the most important indexes for industrial applications. Hence, the effects of GHSV conditions, cycling times, and water vapor on the catalytic oxidation over $PtMn_{0.2}$ @ZSM5 were further investigated. As can be seen in Fig. 12a, there was a decrease of acetone conversion under the same reaction temperature when the GHSV was increased from 30,000 mL/(g·h) (T_{95} = 165 ℃) to 60,000 mL/(g·h) (T_{95} = 210 ℃), which can be related to the shorter retention time of acetone in the catalyst bed. While as the GHSV was increased from 60,000 mL/(g·h) to 75,000 mL/(g·h), the acetone conversion remained unchanged. It indicated an outstanding efficiency of $PtMn_{0.2}$ @ZSM5 for acetone oxidation at high GHSV conditions, which is much required for practical application. After 10 cycles, no loss of catalytic activity was observed over the $PtMn_{0.2}$ @ZSM5 catalyst (Fig. 12b). The TEM result of used $PtMn_{0.2}$ @ZSM5 after 10 cycling tests (Fig. S5)

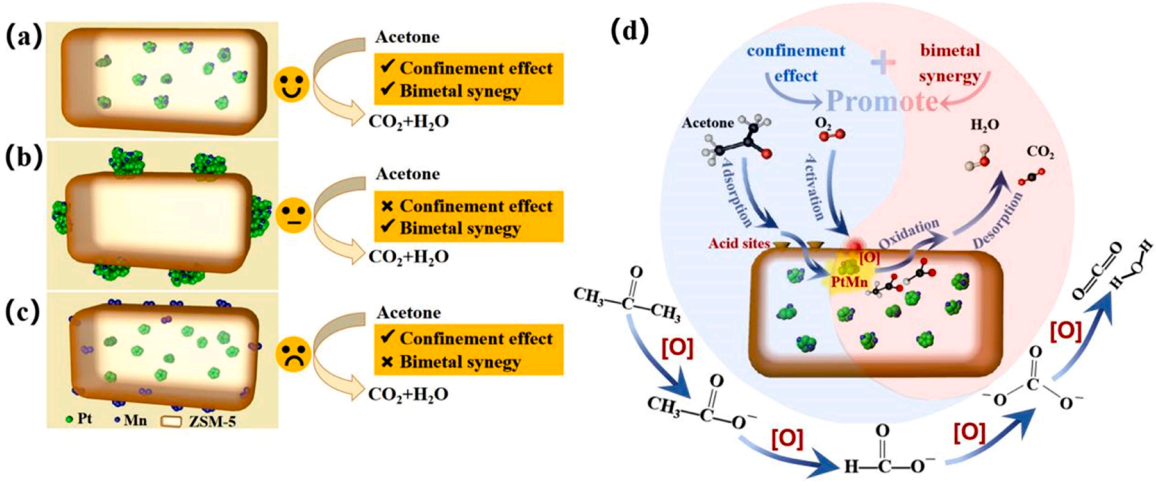

Fig. 11. Schematic illustration of (a) $PtMn_{0.2}$ @ZSM5, (b) $PtMn_{0.2}$/ZSM5, and (c) $Mn_{0.2}$/Pt@ZSM5 catalysts. (d) Schematic illustration of acetone catalytic oxidation over $PtMn_{0.2}$ @ZSM5.

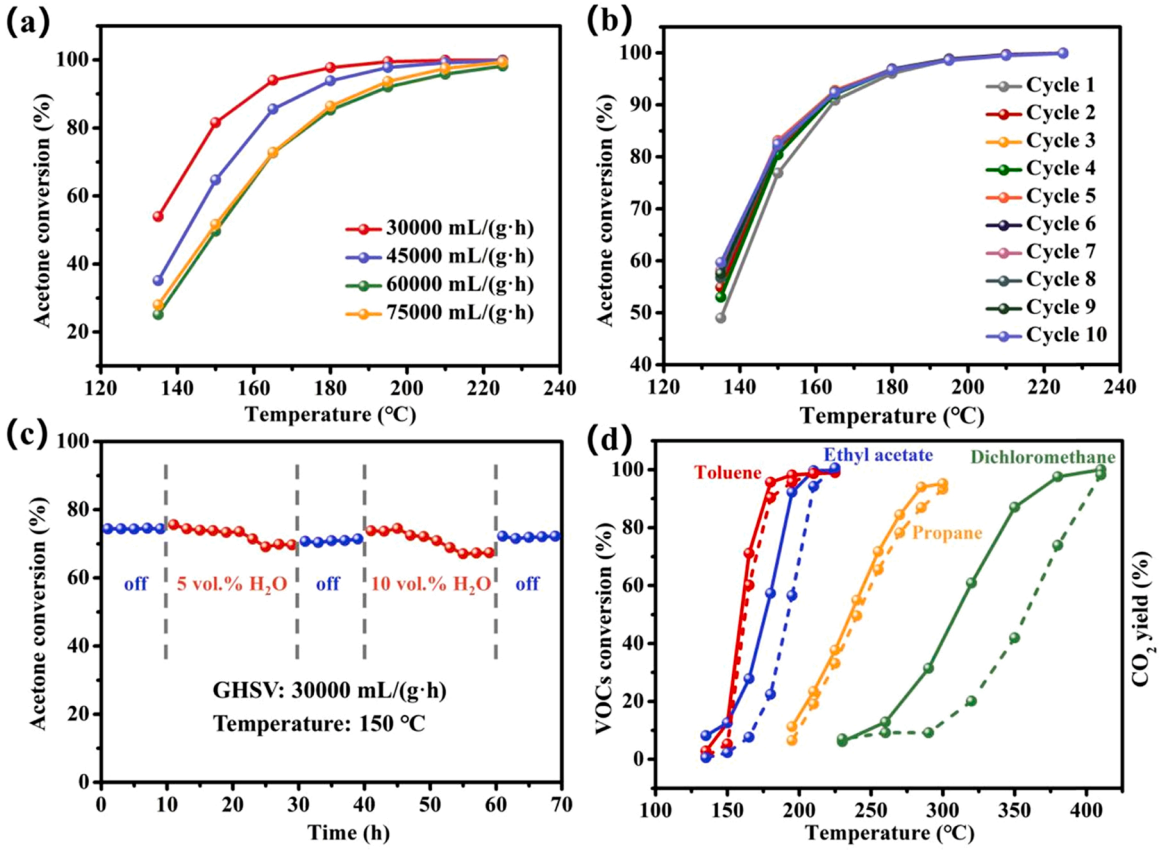

Fig. 12. (a) Effect of GHSV over the $PtMn_{0.2}$ @ZSM5 catalyst. (b) Cycle stability tests over the $PtMn_{0.2}$ @ZSM5 catalyst. (c) Water durability tests over the $PtMn_{0.2}$ @ZSM5 catalyst. (d) Catalytic conversions (solid line) and CO_2 yield (dotted line) of various VOCs over the $PtMn_{0.2}$ @ZSM5 catalyst.

showed that the average size of metal nanoparticles was 6.51 nm, nearly the same as the fresh one (6.42 nm), which highlighted the superior stability and long life of the $PtMn_{0.2}$ @ZSM5 catalyst. Besides, the introduction of water vapor into the reaction system had little effect on the conversion of acetone over the $PtMn_{0.2}$ @ZSM5 catalyst (Fig. 12c), showing a strong tolerance to water vapor.

Furthermore, the catalytic oxidation of other VOCs (toluene, ethyl acetate, propane, and dichloromethane) was also investigated over the $PtMn_{0.2}$ @ZSM5 catalyst (Fig. 12d), and the values of T_{50} and T_{90} were summarized in Table S6. The degradation ability of the $PtMn_{0.2}$ @ZSM5 for different VOCs followed the sequence from easy to difficult: toluene, ethyl acetate, propane, dichloromethane. Among them, the CO_2 yield of toluene, ethyl acetate, and propane had a similar trend with their corresponding conversion, indicating their deep oxidation over the $PtMn_{0.2}$ @ZSM5. But for the catalytic oxidation of dichloromethane, the CO_2 yield was significantly lower than its conversion at lower temperatures. Meanwhile, a small number of CH_3Cl and CO by-products were detected, suggesting incomplete oxidation. These chlorine by-products may cause a toxic effect on the catalyst's active sites, inhibiting further oxidization. When the temperature increased to 410 ℃, the CO_2 yield was up to almost 100%, demonstrating that dichloromethane could be completely oxidized on $PtMn_{0.2}$ @ZSM5 at a higher temperature. Notably, compared with other relevant records, the catalytic performances for these VOCs in this work were all at a higher level [28,52–54], revealing the universal applicability of the catalyst and showing a promising prospect for the elimination of VOCs.

4. Conclusions

In summary, a zeolite-confined bimetal $PtMn_{0.2}$ @ZSM5 catalyst was prepared by direct in-situ synthesis and used for acetone oxidation. It exhibited remarkable catalytic activity (T_{95} = 165 ℃) attributed to the confinement effect of zeolite and the appropriate synergy effect of bimetallic components. The $PtMn_{0.2}$ @ZSM5 presented a smaller nanoparticle size, more abundant acid sites, higher active Pt^0 proportion, and sufficient active oxygen species. As a result, the acetone adsorption, gas-phase oxygen activation, acetone deep oxidation, and CO_2 desorption were facilitated, significantly promoting the catalytic oxidation of acetone following the L-H mechanism. Moreover, the $PtMn_{0.2}$ @ZSM5 presented good cycling stability, water resistance, and broad VOC applicability, promising practical industrial application prospects.

CRediT authorship contribution statement

Lizhe Yang: Conceptualization, Methodology, Investigation, Writing – original draft. **Qingling Liu:** Supervision, Funding acquisition, Resources. **Rui Han:** Supervision, Funding acquisition, Writing – review & editing. **Kaixuan Fu:** Validation. **Yun Su:** Validation. **Yanfei Zheng:** Visualization. **Xueqian Wu:** Visualization. **Chunfeng Song:** Writing – review & editing. **Na Ji:** Writing – review & editing. **Xuebin Lu:** Writing – review & editing. **Degang Ma:** Writing – review & editing.

Declaration of Competing Interest

The authors declare that they have no known competing financial interests or personal relationships that could have appeared to influence the work reported in this paper.

Acknowledgments

The work was supported by the National Key Research and

Development Program of China (2019YFC1904100, 2019YFC1904102, 2019YFC1903902); the National Engineering Laboratory for Mobile Source Emission Control Technology of China (NELMS2017A03); the Natural National Science Foundation of China (No. 21503144, No. 21690083); Tianjin Research Program of Ecological Environmental Treatment (No. 18ZXSZSF00210, No. 18ZXSZSF00060); the Tianjin Research Program of Application Foundation and Advanced Technique (No. 15JCQNJC08500, No. 16JCQNJC05400).

Appendix A. Supporting information

Supplementary data associated with this article can be found in the online version at doi:10.1016/j.apcatb.2022.121224.

References

[1] C. Yang, G. Miao, Y. Pi, Q. Xia, J. Wu, Z. Li, J. Xiao, Abatement of various types of VOCs by adsorption/catalytic oxidation: a review, Chem. Eng. J. 370 (2019) 1128–1153, https://doi.org/10.1016/j.cej.2019.03.232.

[2] C. He, J. Cheng, X. Zhang, M. Douthwaite, S. Pattisson, Z.P. Hao, Recent advances in the catalytic oxidation of volatile organic compounds: a review based on pollutant sorts and sources, Chem. Rev. 119 (7) (2019) 4471–4568, https://doi.org/10.1021/acs.chemrev.8b00408.

[3] Y. Guo, M. Wen, G. Li, T. An, Recent advances in VOC elimination by catalytic oxidation technology onto various nanoparticles catalysts: a critical review, Appl. Catal. B Environ. 281 (2021), 119447, https://doi.org/10.1016/j.apcatb.2020.119447.

[4] S. Lu, Q. Liu, R. Han, J. Shi, M. Guo, C. Song, N. Ji, X. Lu, D. Ma, Core-shell structured Y zeolite/hydrophobic organic polymer with improved toluene adsorption capacity under dry and wet conditions, Chem. Eng. J. 409 (2021), 128194, https://doi.org/10.1016/j.cej.2020.128194.

[5] S. Li, X. Dang, X. Yu, G. Abbas, Q. Zhang, L. Cao, The application of dielectric barrier discharge non-thermal plasma in VOCs abatement: a review, Chem. Eng. J. 388 (2020), 124275, https://doi.org/10.1016/j.cej.2020.124275.

[6] S. Lu, Q. Liu, R. Han, M. Guo, J. Shi, C. Song, N. Ji, X. Lu, D. Ma, Potential applications of porous organic polymers as adsorbent for the adsorption of volatile organic compounds, J. Environ. Sci. 105 (2021) 184–203, https://doi.org/10.1016/j.jes.2021.01.007.

[7] Y. Zheng, Q. Zhao, C. Shan, S. Lu, Y. Su, R. Han, C. Song, N. Ji, D. Ma, Q. Liu, Enhanced acetone oxidation over the CeO_2/Co_3O_4 catalyst derived from metal–organic frameworks, ACS Appl. Mater. Interfaces 12 (25) (2020) 28139–28147, https://doi.org/10.1021/acsami.0c04904.

[8] Z. Wang, P. Ma, K. Zheng, C. Wang, Y. Liu, H. Dai, C. Wang, H.-C. Hsi, J. Deng, Size effect, mutual inhibition and oxidation mechanism of the catalytic removal of a toluene and acetone mixture over TiO_2 nanosheet-supported Pt nanocatalysts, Appl. Catal. B Environ. 274 (2020), 118963, https://doi.org/10.1016/j.apcatb.2020.118963.

[9] T. Kondratowicz, M. Drozdek, M. Michalik, W. Gac, M. Gajewska, P. Kuśtrowski, Catalytic activity of Pt species variously dispersed on hollow ZrO_2 spheres in combustion of volatile organic compounds, Appl. Surf. Sci. 513 (2020), 145788, https://doi.org/10.1016/j.apsusc.2020.145788.

[10] C. Chen, F. Chen, L. Zhang, S. Pan, C. Bian, X. Zheng, X. Meng, F.-S. Xiao, Importance of platinum particle size for complete oxidation of toluene over Pt/ZSM-5 catalysts, Chem. Commun. 51 (27) (2015) 5936–5938, https://doi.org/10.1039/C4CC09383F.

[11] Y. Ge, K. Fu, Q. Zhao, N. Ji, C. Song, D. Ma, Q. Liu, Performance study of modified Pt catalysts for the complete oxidation of acetone, Chem. Eng. Sci. 206 (2019) 499–506, https://doi.org/10.1016/j.ces.2019.05.051.

[12] M. Juneau, R. Liu, Y. Peng, A. Malge, Z. Ma, M.D. Porosoff, Characterization of metal-zeolite composite catalysts: determining the environment of the active phase, ChemCatChem 12 (7) (2020) 1826–1852, https://doi.org/10.1002/cctc.201902039.

[13] C. Dong, Y. Li, D. Cheng, M. Zhang, J. Liu, Y.-G. Wang, D. Xiao, D. Ma, Supported metal clusters: fabrication and application in heterogeneous catalysis, ACS Catal. 10 (19) (2020) 11011–11045, https://doi.org/10.1021/acscatal.0c02818.

[14] T.W. Hansen, A.T. DeLaRiva, S.R. Challa, A.K. Datye, Sintering of catalytic nanoparticles: particle migration or Ostwald Ripening? Acc. Chem. Res. 46 (8) (2013) 1720–1730, https://doi.org/10.1021/ar3002427.

[15] S.-M. Wu, X.-Y. Yang, C. Janiak, Confinement effects in zeolite-confined noble metals, Angew. Chem. Int. Ed. 58 (36) (2019) 12340–12354, https://doi.org/10.1002/anie.201900013.

[16] L. Liu, U. Díaz, R. Arenal, G. Agostini, P. Concepción, A. Corma, Generation of subnanometric platinum with high stability during transformation of a 2D zeolite into 3D, Nat. Mater. 16 (1) (2017) 132–138, https://doi.org/10.1038/nmat4757.

[17] H.J. Cho, D. Kim, J. Li, D. Su, B. Xu, Zeolite-encapsulated Pt nanoparticles for tandem catalysis, J. Am. Chem. Soc. 140 (41) (2018) 13514–13520, https://doi.org/10.1021/jacs.8b09568.

[18] R. Yan, S. Lin, Y. Li, W. Liu, Y. Mi, C. Tang, L. Wang, P. Wu, H. Peng, Novel shielding and synergy effects of Mn-Ce oxides confined in mesoporous zeolite for low temperature selective catalytic reduction of NOx with enhanced SO_2/H_2O tolerance, J. Hazard. Mater. 396 (2020), 122592, https://doi.org/10.1016/j.jhazmat.2020.122592.

[19] L. Liu, A. Corma, Confining isolated atoms and clusters in crystalline porous materials for catalysis, Nat. Rev. Mater. 6 (3) (2021) 244–263, https://doi.org/10.1038/s41578-020-00250-3.

[20] L. Liu, M. Lopez-Haro, C. Lopes, C. Li, P. Concepcion, L. Simonelli, J.J. Calvino, A. Corma, Regioselective generation and reactivity control of subnanometric platinum clusters in zeolites for high-temperature catalysis, Nat. Mater. 18 (2019), https://doi.org/10.1038/s41563-019-0412-6.

[21] T.-L. Cui, W.-Y. Ke, W.-B. Zhang, H.-H. Wang, X.-H. Li, J.-S. Chen, Encapsulating palladium nanoparticles inside mesoporous MFI zeolite nanocrystals for shape-selective catalysis, Angew. Chem. Int. Ed. 55 (32) (2016) 9178–9182, https://doi.org/10.1002/anie.201602429.

[22] Q. Sun, N. Wang, T. Zhang, R. Bai, A. Mayoral, P. Zhang, Q. Zhang, O. Terasaki, J. Yu, Zeolite-encaged single-atom rhodium catalysts: highly-efficient hydrogen generation and shape-selective tandem hydrogenation of nitroarenes, Angew. Chem. Int. Ed. 58 (51) (2019) 18570–18576, https://doi.org/10.1002/anie.201912367.

[23] Y. Su, K. Fu, Y. Zheng, N. Ji, C. Song, D. Ma, X. Lu, R. Han, Q. Liu, Catalytic oxidation of dichloromethane over Pt-Co/HZSM-5 catalyst: synergistic effect of single-atom Pt, Co_3O_4, and HZSM-5, Appl. Catal. B Environ. 288 (2021), 119980, https://doi.org/10.1016/j.apcatb.2021.119980.

[24] K. Zhang, L. Dai, Y. Liu, J. Deng, L. Jing, K. Zhang, Z. Hou, X. Zhang, J. Wang, Y. Feng, Y. Zhang, H. Dai, Insights into the active sites of chlorine-resistant Pt-based bimetallic catalysts for benzene oxidation, Appl. Catal. B Environ. 279 (2020), 119372, https://doi.org/10.1016/j.apcatb.2020.119372.

[25] J. Kim, J.E. Lee, H.W. Lee, J.-K. Jeon, J. Song, S.-C. Jung, Y.F. Tsang, Y.-K. Park, Catalytic ozonation of toluene using Mn–M bimetallic HZSM-5 (M: Fe, Cu, Ru, Ag) catalysts at room temperature, J. Hazard. Mater. 397 (2020), 122577, https://doi.org/10.1016/j.jhazmat.2020.122577.

[26] Y. Zheng, Q. Liu, C. Shan, Y. Su, K. Fu, S. Lu, R. Han, C. Song, N. Ji, D. Ma, Defective ultrafine MnOx nanoparticles confined within a carbon matrix for low-temperature oxidation of volatile organic compounds, Environ. Sci. Technol. 55 (8) (2021) 5403–5411, https://doi.org/10.1021/acs.est.0c08335.

[27] Q. Zhao, Y. Ge, K. Fu, Y. Zheng, Q. Liu, C. Song, N. Ji, D. Ma, Catalytic performance of the Pd/TiO_2 modified with MnO_x catalyst for acetone total oxidation, Appl. Surf. Sci. 496 (2019), 143579, https://doi.org/10.1016/j.apsusc.2019.143579.

[28] T. Dong, W. Liu, M. Ma, H. Peng, S. Yang, J. Tao, C. He, L. Wang, P. Wu, T. An, Hierarchical zeolite enveloping $Pd\text{-}CeO_2$ nanowires: an efficient adsorption/catalysis bifunctional catalyst for low temperature propane total degradation, Chem. Eng. J. 393 (2020), 124717, https://doi.org/10.1016/j.cej.2020.124717.

[29] H. Wang, L. Wang, F.-S. Xiao, Metal@Zeolite hybrid materials for catalysis, ACS Cent. Sci. 6 (10) (2020) 1685–1697, https://doi.org/10.1021/acscentsci.0c01130.

[30] T. Otto, S.I. Zones, E. Iglesia, Challenges and strategies in the encapsulation and stabilization of monodisperse Au clusters within zeolites, J. Catal. 339 (2016) 195–208, https://doi.org/10.1016/j.jcat.2016.04.015.

[31] A. Chen, W. Zhang, X. Li, D. Tan, X. Han, X. Bao, One-pot encapsulation of Pt nanoparticles into the mesochannels of SBA-15 and their catalytic dehydrogenation of methylcyclohexane, Catal. Lett. 119 (1) (2007) 159–164, https://doi.org/10.1007/s10562-007-9214-6.

[32] Q. Sun, B.W.J. Chen, N. Wang, Q. He, A. Chang, C.-M. Yang, H. Asakura, T. Tanaka, M.J. Hulsey, C.-H. Wang, J. Yu, N. Yan, Zeolite-encaged Pd-Mn nanocatalysts for CO_2 hydrogenation and formic acid dehydrogenation, Angew. Chem. Int. Ed. 59 (45) (2020) 20183–20191, https://doi.org/10.1002/anie.202008962.

[33] X. Fan, D. Liu, X. Sun, X. Yu, D. Li, Y. Yang, H. Liu, J. Diao, Z. Xie, L. Kong, X. Xiao, Z. Zhao, Mn-doping induced changes in Pt dispersion and Pt_xMn_y alloying extent on Pt/Mn-DMSN catalyst with enhanced propane dehydrogenation stability, J. Catal. 389 (2020) 450–460, https://doi.org/10.1016/j.jcat.2020.06.016.

[34] T.-S. Kim, J. Kim, H.C. Song, D. Kim, B. Jeong, J. Lee, J.W. Shin, R. Ryoo, J.Y. Park, Catalytic synergy on PtNi bimetal catalysts driven by interfacial intermediate structures, ACS Catal. 10 (18) (2020) 10459–10467, https://doi.org/10.1021/acscatal.0c02467.

[35] P.-P. Zhao, J. Chen, H.-B. Yu, B.-H. Cen, W.-Y. Wang, M.-F. Luo, J.-Q. Lu, Insights into propane combustion over MoO_3 promoted Pt/ZrO_2 catalysts: the generation of $Pt\text{-}MoO_3$ interface and its promotional role on catalytic activity, J. Catal. 391 (2020) 80–90, https://doi.org/10.1016/j.jcat.2020.08.012.

[36] H. Jeong, D. Shin, B.-S. Kim, J. Bae, S. Shin, C. Choe, J.W. Han, H. Lee, Controlling the oxidation state of Pt single atoms for maximizing catalytic activity, Angew. Chem. Int. Ed. 59 (46) (2020) 20691–20696, https://doi.org/10.1002/anie.202009776.

[37] J. Chen, M. Jiang, W. Xu, J. Chen, Z. Hong, H. Jia, Incorporating Mn cation as anchor to atomically disperse Pt on TiO_2 for low-temperature removal of formaldehyde, Appl. Catal. B Environ. 259 (2019), 118013, https://doi.org/10.1016/j.apcatb.2019.118013.

[38] Z. Shi, P. Yang, F. Tao, R. Zhou, New insight into the structure of CeO_2–TiO_2 mixed oxides and their excellent catalytic performances for 1,2-dichloroethane oxidation, Chem. Eng. J. 295 (2016) 99–108, https://doi.org/10.1016/j.cej.2016.03.032.

[39] H. Huang, C. Zhang, L. Wang, G. Li, L. Song, G. Li, S. Tang, X. Li, Promotional effect of HZSM-5 on the catalytic oxidation of toluene over MnO_x/HZSM-5 catalysts, Catal. Sci. Technol. 6 (12) (2016) 4260–4270, https://doi.org/10.1039/C5CY02011E.

[40] J. He, D. Chen, N. Li, Q. Xu, H. Li, J. He, J. Lu, Controlled fabrication of mesoporous ZSM-5 zeolite-supported PdCu alloy nanoparticles for complete oxidation of toluene, Appl. Catal. B Environ. 265 (2020), 118560, https://doi.org/10.1016/j.apcatb.2019.118560.

[41] J. Chen, X. Chen, D. Yan, M. Jiang, W. Xu, H. Yu, H. Jia, A facile strategy of enhancing interaction between cerium and manganese oxides for catalytic removal of gaseous organic contaminants, Appl. Catal. B Environ. 250 (2019) 396–407, https://doi.org/10.1016/j.apcatb.2019.03.042.

[42] T. Gan, X. Chu, H. Qi, W. Zhang, Y. Zou, W. Yan, G. Liu, Pt/Al_2O_3 with ultralow Pt-loading catalyze toluene oxidation: promotional synergistic effect of Pt nanoparticles and Al_2O_3 support, Appl. Catal. B Environ. 257 (2019), 117943, https://doi.org/10.1016/j.apcatb.2019.117943.

[43] S. Cai, D. Zhang, L. Zhang, L. Huang, H. Li, R. Gao, L. Shi, J. Zhang, Comparative study of 3D ordered macroporous $Ce_{0.75}Zr_{0.2}M_{0.05}O_{2-\delta}$ (M = Fe, Cu, Mn, Co) for selective catalytic reduction of NO with NH_3, Catal. Sci. Technol. 4 (1) (2014) 93–101, https://doi.org/10.1039/C3CY00398A.

[44] X. Weng, P. Sun, Y. Long, Q. Meng, Z. Wu, Catalytic oxidation of chlorobenzene over $Mn_xCe_{1-x}O_2$/HZSM-5 catalysts: a study with practical implications, Environ. Sci. Technol. 51 (14) (2017) 8057–8066, https://doi.org/10.1021/acs.est.6b06585.

[45] S. Rong, P. Zhang, F. Liu, Y. Yang, Engineering crystal facet of α-MnO_2 nanowire for highly efficient catalytic oxidation of carcinogenic airborne formaldehyde, ACS Catal. 8 (4) (2018) 3435–3446, https://doi.org/10.1021/acscatal.8b00456.

[46] W. Yang, Za Su, Z. Xu, W. Yang, Y. Peng, J. Li, Comparative study of α-, β-, γ- and δ-MnO_2 on toluene oxidation: oxygen vacancies and reaction intermediates, Appl. Catal. B Environ. 260 (2020), 118150, https://doi.org/10.1016/j.apcatb.2019.118150.

[47] H. Luo, X.-D. Wu, D. Weng, S. Liu, R. Ran, A novel insight into enhanced propane combustion performance on PtUSY catalyst, Rare Met. 36 (1) (2017) 1–9, https://doi.org/10.1007/s12598-016-0760-1.

[48] X. Wu, L. Zhang, D. Weng, S. Liu, Z. Si, J. Fan, Total oxidation of propane on Pt/WOx/Al_2O_3 catalysts by formation of metastable $Pt^{\delta+}$ species interacted with WO_x clusters, J. Hazard. Mater. 225–226 (2012) 146–154, https://doi.org/10.1016/j.jhazmat.2012.05.011.

[49] Y. Shi, Z. Li, J. Wang, R. Zhou, Synergistic effect of Pt/Ce and USY zeolite in Pt-based catalysts with high activity for VOCs degradation, Appl. Catal. B Environ. 286 (2021), 119936, https://doi.org/10.1016/j.apcatb.2021.119936.

[50] M. El-Maazawi, A.N. Finken, A.B. Nair, V.H. Grassian, Adsorption and photocatalytic oxidation of acetone on TiO2: an in situ transmission FT-IR study, J. Catal. 191 (1) (2000) 138–146, https://doi.org/10.1006/jcat.1999.2794.

[51] W. Su, J. Zhang, Z. Feng, T. Chen, P. Ying, C. Li, Surface phases of TiO2 nanoparticles studied by UV Raman spectroscopy and FT-IR spectroscopy, J. Phys. Chem. C 112 (20) (2008) 7710–7716, https://doi.org/10.1021/jp7118422.

[52] C. Chen, J. Zhu, F. Chen, X. Meng, X. Zheng, X. Gao, F.-S. Xiao, Enhanced performance in catalytic combustion of toluene over mesoporous Beta zeolite-supported platinum catalyst, Appl. Catal. B Environ. 140–141 (2013) 199–205, https://doi.org/10.1016/j.apcatb.2013.03.050.

[53] O.S.G.P. Soares, R.P. Rocha, J.J.M. Órfão, M.F.R. Pereira, J.L. Figueiredo, Ethyl and butyl acetate oxidation over manganese oxides, Chin. J. Catal. 39 (1) (2018) 27–36, https://doi.org/10.1016/S1872-2067(17)62986-3.

[54] Z. El Assal, S. Ojala, S. Pitkäaho, L. Pirault-Roy, B. Darif, J.-D. Comparot, M. Bensitel, R.L. Keiski, R. Brahmi, Comparative study on the support properties in the total oxidation of dichloromethane over Pt catalysts, Chem. Eng. J. 313 (2017) 1010–1022, https://doi.org/10.1016/j.cej.2016.10.139.